"Involta" Ilmiy Jurnali

Vebsayt: https://involta.uz/

PROCESS OF NANOCARBON REMOVAL FROM METHANE IN THE PARTICIPATION OF $(CuO)_x*(CoO)_y*(NiO)_z*(Fe_2O_3)_k*(MoO_3)_m$/HSZ CATALYST

Khilola N. Kholmirzayeva[1],

Normurot I. Fayzullayev[2]

Doctoral student, Department of Physical and Colloid Chemistry, Samarkand State University, Blv. 15, Samarkand, Uzbekistan

ORCiD: https://orcid.org/0000-0002-4772-3674

[#2]DSc, Professor, Department of Polymer Chemistry and Chemical Technology, Samarkand State University Blv. 15, Samarkand, Uzbekistan

ORCiD: https://orcid.org/0000-0001-5838-3743

[1]hilola.xolmirzaeva@mail.ru,

[2]f-normurot@samdu.uz

ABSTRACT

The process of nanocarbon of methane from methane was carried out in the presence of $(CuO)_x*(CoO)_y*(NiO)_z*(Fe_2O_3)_k*(MoO_3)_m$/HSZ catalyst: The essence of the method is the interaction of nitrate mixtures of metals included in the

catalyst and the organic matter in the air at temperatures ≥500 ℃. The reaction is followed by the formation of finely dispersed oxides of metals. It allows calculating the concentration of system components not only at the outlet of the apparatus, but also along the length of the reactor. As a result, the methane supplied to the surface of the catalyst manages to interact with it before methane escapes with a stream of the initial gas mixture. The kinetic curves of the time dependence of the change in the specific amount of carbon in the catalyst do not have an induction period at all. The process temperature did not change and was 650 ℃. Thus, real experiments were repeated using computer technology. The peculiarity of the nanocarbon production process is that the catalyst is consumed during the process.

Keywords: reactor, catalyst, methane, nanocarbon, modeling, optimization.

INTRODUCTION

To date, there has been a growing demand for effective, environmentally safe adsorbents in various sectors of the economy, including machinery and technology, including pharmaceuticals, petroleum, cosmetology, oil, and gas refining industries [1-5]. In addition, the properties of the obtained products and the nature of the surface centers of the catalysts have been studied in several studies [6]. The influence of various factors on the synthesis of nanocarbon from walnut peel, apricot kernel, methane, natural gas, and propane-butane fractions was studied, and the texture and sorption characteristics of the obtained nanocarbon were examined. The catalytic activity of the catalyst containing $(CuO)_x*(CoO)_y*(NiO)_z*(Fe_2O_3)_k*(MoO_3)_m$/HSZ prepared on the basis of "zol-gel" technology for the implementation of processes was studied under differential reactor conditions. At the same time, the effect of various factors on the rate of formation of nanocarbon obtained from methane, natural gas, and propane-butane fractions was studied and optimal process conditions were proposed [7-10]. The physicochemical and operational properties of two industrial catalysts for nanocarbon synthesis were analyzed. Different methods: X-ray phase, chemical,

and IR spectroscopy studied the composition of catalysts [11-12].

Thermocatalytic decomposition (TCD) of methane is being studied as a method of converting natural gas to hydrogen and functional carbon. In these processes, carbon is usually formed over the catalyst phase, leading to the growth of particles. Therefore, the development of a particle growth model is necessary to understand the thermocatalytic decomposition limitations of methane and to evaluate the optimal parameters and process conditions. A Multi-Grain Model (MGM) has been used to combine the effects of particle growth, kinetics, and internal heat and mass transfer [13 -15]. Methane conversion in the reactor is calculated as a function of the longitudinal coordinate, temperature, and specific gas and catalyst flow rate of the specific carbon content and relative catalyst activity. At the specified specific methane flow rate, it is shown that there is an optimal specific catalyst flow with the maximum specific yield of carbon nanotubes, where in the combined reactor this efficiency is higher than in the countercurrent reactor [16-18]. Based on laboratory-scale experimental data, low losses (less than 10%) are achieved based on laboratory-scale experimental data. In general, the work leads to the introduction of detailed kinetics in the simulation of industrial liquefied reactors [19, 20].

EXPERIMENTAL PART

The extraction of nanocarbons from methane ($Fe_2(MoO_4)_3$*MoO_3) (cat №1) and $(CuO)_x$*$(CoO)_y$*$(NiO)_z$*$(Fe_2O_3)_k$*$(MoO_3)_m$/HSZ (cat №2) The catalyst containing $(CuO)_x$*$(CoO)_y$*$(NiO)_z$*$(Fe_2O_3)_k$*$(MoO_3)_m$/HSZ turned out to be more active compared to the previous layer №1, and experiments with it were carried out in a much lower temperature range.

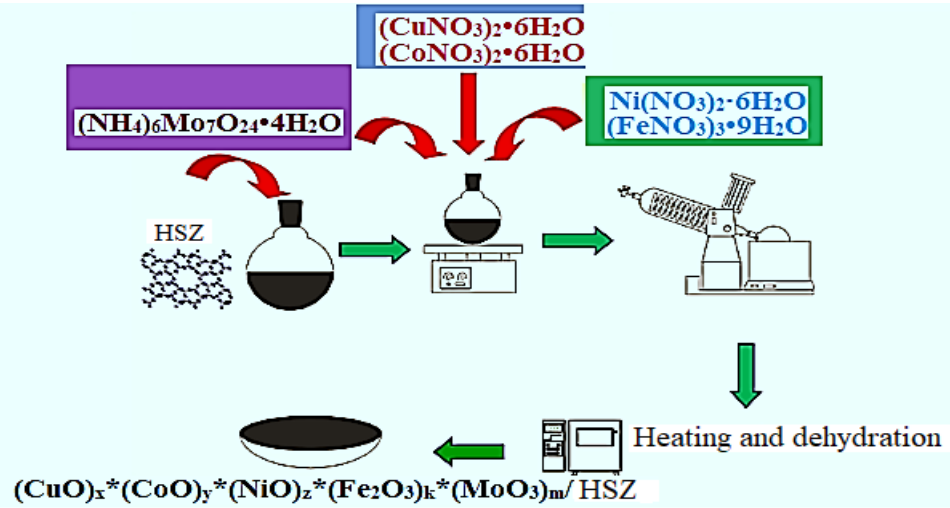

Figure 1. Scheme of preparation of catalyst containing $(CuO)_x*(CoO)_y*(NiO)_z*(Fe_2O_3)_k*(MoO_3)_m$/HSZ

The essence of the method is the interaction of nitrate mixtures of metals included in the catalyst and the organic matter in the air at temperatures ≥500 ℃. The reaction is followed by the formation of finely dispersed oxides of metals.

The equations for changing the concentration of gas phase components have the following form:

$$\frac{\partial C_i}{\partial t} + v_1 \frac{\partial C_i}{\partial x} = D_i \frac{\partial^2 C_i}{\partial x^2} + \tilde{J}_i \qquad (1)$$

where is v_1–the linear velocity of the gas mixture, m /s; C_i - concentration of the i-component of the gas phase (i = 1 ... 3), mol/m^3; D_i- diffusion coefficient of the i-component of the gas phase, m^2 /s; $\tilde{J}_i$ - rate of formation or consumption of i-component according to the reactions that occur on the surface of the catalyst, mol / (m^{3}s); t - time, c; x - longitudinal coordinate of the reactor, m (counting head for the x axis - the point of entry of the gas phase into the apparatus).

The initial conditions of equation (1) are as follows:

$$C_i(t = 0, x) = C_i^0(x) \qquad (2)$$

(2) states that the values of concentrations for each component of the gas phase at each point of the reactor at the initial moment of time are known.

The boundary conditions of equation (1) take into account the flow of reagents into the apparatus together with the initial gas mixture:

$$\begin{cases} C_i(x=0) = C_i^{кир} \\ \frac{\partial C_i}{\partial x}|_{x=l_{апп}} = 0 \end{cases} \quad (3)$$

Where l_{app} - device length, m; C_i - initial gas component concentration at reactor inlet, mol / m3. The equations for changing the concentration of the dispersed phase components are written as follows:

$$\frac{\partial \tilde{C}_i}{\partial t} - v_2 \frac{\partial \tilde{C}_i}{\partial x} = \tilde{J}_i \quad (4)$$

Where is $\tilde{C}_i$ – the surface concentration of the solid phase component per unit mass of the catalyst, mol / kg; $\tilde{J}_i$ - the rate of formation or consumption of the i-component of the dispersed phase based on the reactions that occur on the catalyst's surface, mol / (kg ·s); v_2 – the linear velocity of the dispersed phase, m /s (the minus sign indicates that the continuous and dispersed phases move in opposite current).

The initial conditions for solving equation (4) are written as follows:

$$\tilde{C}_i(t=0,x) = \tilde{C}_i^0(x) \quad (5)$$

This is $\tilde{C}_i^0(x)$ −the distribution of the i-component concentration of the dispersed phase along the length of the apparatus at the initial moment of time, mol /kg.

In addition, to solve equation (4), it is necessary to have boundary conditions:

$$\begin{cases} \tilde{C}_i(x=l) = \tilde{C}_i^{кир} \\ \frac{\partial \tilde{C}_i}{\partial x}|_{x=0} = 0 \end{cases} \quad (6)$$

where is $\tilde{C}_i^{inlet}$ – the surface concentration of the dispersed phase component at the reactor inlet, mol /kg.

Catalyst mass equilibrium equation:

$$\frac{\partial m_{Kt}}{\partial t} - v_2 \frac{\partial m_{Kt}}{\partial x} = 0 \quad (7)$$

where is m_{Kt} −the mass of the catalyst, kg.

The initial conditions of equation (7) determine the mass distribution of the catalyst at time t = 0:

$$m_{Kt}(t=0,x) = m_{Kt}^0(x) \quad (8)$$

The boundary conditions of equation (7) are written as follows:

$$\begin{cases} m_{Kt}(x = l) = m_{Kt}^{\text{кир}} \\ \frac{\partial m_{Kt}}{\partial x}|_{x=0} = 0 \end{cases}$$

(9)

where m_{Kt}^{inlet}- the mass of the catalyst at the entrance to the reactor, kg.

These mathematical models (1) -(9) allow one to calculate the concentration of system components not only at the outlet of the apparatus, but also along the length of the reactor.

EXPERIMENTAL RESULTS AND THEIR DISCUSSION

This can be explained by the much higher activity of cat №2, which provides much higher rates of reactions in the catalyst. As a result, the methane supplied to the surface of the catalyst manages to interact with it before methane escapes with a stream of initial gas mixture.

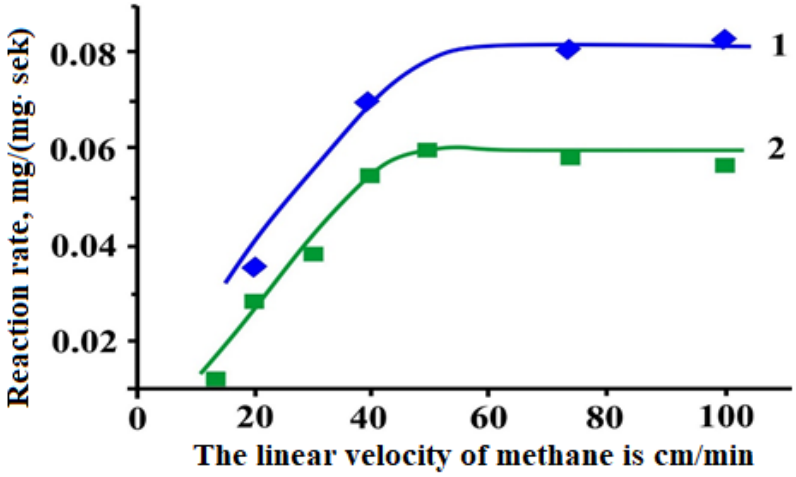

Figure 3. At 25 minutes after the start of the experiment, the average rate of the nanocarbon synthesis reaction on the cat №2 catalyst was different at different temperatures: 1-600 °C; 2-650 °C Dependence on the linear velocity of methane

As can be seen from Figure 3, the process must be carried out at linear velocities of not less than 25 cm /min of the initial gas mixture flow. Subsequent studies were performed on methane at a linear velocity of 35 cm /min.

The results of the study of the effect of temperature on the rate of nanocarbon synthesis showed that cat №2 differs from cat №1 in catalyst. The application of cat №2 at lower temperatures allows nanocarbon to be obtained with

a much higher specific yield, while the change in the specific amount of carbon in the catalyst is time-dependent and the kinetic curves have no induction period at all. The results of the experimental measurements are shown in Figure 4.

The micro-images of the product obtained at a linear velocity of 35 cm /min of methane 2 hours after the start of the experiment at a temperature of 560 ℃ in a 10 mg solution of cat №2 catalyst are given in Figure 5. As can be seen, the product mainly represents nanocarbon with a diameter of 10 to 60 nm and a purity of about 98%. The image was obtained using an electron microscope, JEM-1400 (JEOL, Japan).

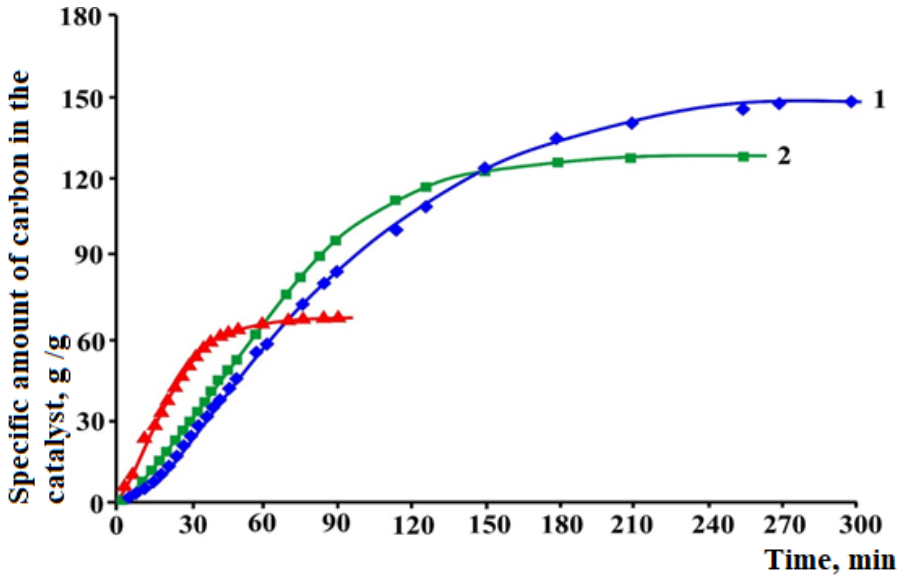

Figure 4. Cat №2 in the catalyst at various temperatures over time: 1 - 560 ℃; 2 – 580^{0}C; 3 - 680 ℃ Change in the specific gravity of nanocarbon derived from methane

Figure 4 shows a graph of the change in temperature $(CuO)_x*(CoO)_y*(NiO)_z*(Fe_2O_3)_k*(MoO_3)_m$/HSZ (cat №2) at different temperatures over time as the catalyst increases. At 560 300 for 300 min, the catalyst exhibits its highest activity. At 560^{o}C, the specific amount of carbon in the catalyst is 150 g /g. However, as the temperature rises (680^{o}C), the specific gravity of the nanocarbon decreases sharply (68 g /g).

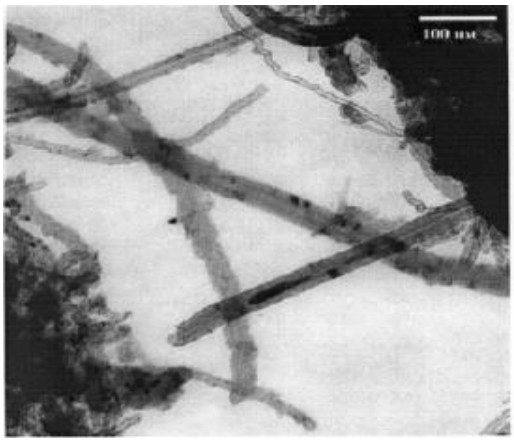

Figure 5. Micro-image of pyrolysis product of methane on cat №2 catalyst (temperature 560 °C, catalyst mass 10 mg, methane linear velocity 35 cm /min)

Mathematical modeling of a methane catalytic pyrolysis continuous operating reactor. At present, there is almost no doubt that in the near future, the industry will need to produce high-yield and low-cost production of methane-derived nanocarbon. In this connection, the reaction of organizing the synthesis of methane-derived nanocarbon in a continuous mode seems very promising. This approach, in our opinion, improves the efficiency of these devices and, at the same time, reduces the cost of the finished product, methane-derived nanocarbon. To confirm these assumptions, it was decided to use a kinetic scheme of nanocarbon formation in the calculation of a continuously operating methane pyrolysis reactor (Table 1).

Table 1

Kinetic constants of the model in cat №2 catalysts in mathematical modeling of the methane pyrolysis reactor

№ stages	cat №2	
	$\tilde{k}_j^0$	$\widetilde{E}_J$ kJ/mol
1. $K_t + CH_4 \rightarrow [CH_3 - K_t] + H$	$3{,}6 \cdot 10^{-2}$	56,6
2.$[CH_3 - K_t] + H \rightarrow [CH_2 - K_t] + H_2$	425	10,0
3.$[CH_2 - K_t] + H \rightarrow [CH - K_t] + H_2$	425	10,0
4.$[CH - K_t] + H \rightarrow [C - K_t] + H_2$	425	10,0

5.$[C-K_t] \rightarrow C_{\text{нт}} + K_t$	$6{,}5 \cdot 10^5$	5,1
6.$[C-K_t] \rightarrow C_A + K_t$	$3{,}4 \cdot 10^5$	54,5
7.$K_t + H_2 \rightarrow [H-K_t] + H$	6,15	64,1
8.$[H-K_t] + H \rightarrow K_t + H_2$	9,23	60,3

The continuous operation mode of the methane catalytic pyrolysis reactor is achieved by moving the catalyst layer along the device length with a countercurrent flow relative to the gas phase.

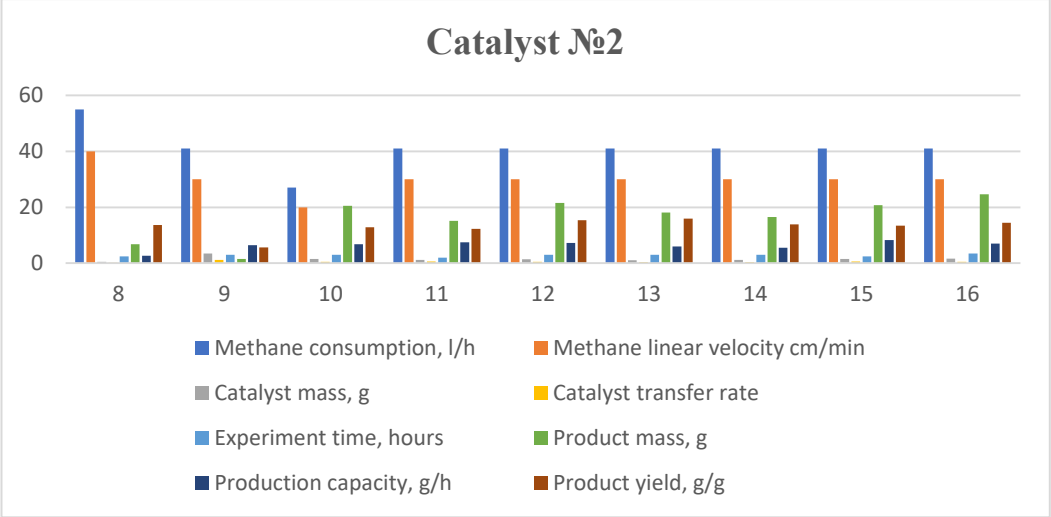

Figure 6. Results of experimental studies of catalyst in a continuous reactor (reactor temperature, 600 ℃)

The diameter of the reactor is 54 mm and the length of the heated part is 300 mm. The process temperature remained constant at 650 °C. The linear velocity of the gas supply (or its flow rate) as well as the catalyst flow rate were varied. Thus, real experiments were repeated using computer technology. The results of the calculations were compared with the experimental data, and the mathematical model developed demonstrated a good correlation between the experimental and calculated data in a continuous reactor using the kinetic constants selected for the reactor (Figure 6).

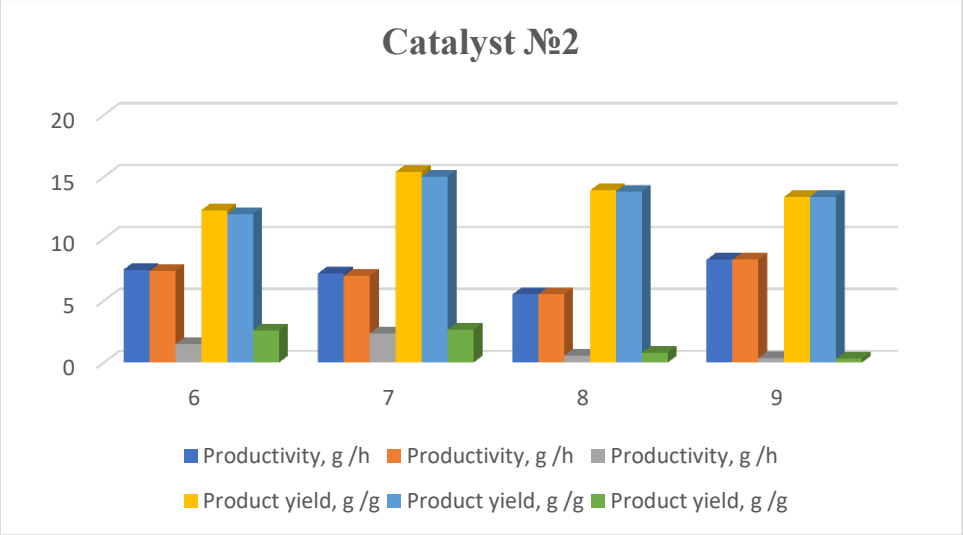

Figure 7. Comparison of the results of mathematical modeling of a continuous reactor with experimental data (process temperature of 650 °C)

As shown in Figure 7, the best result in the presence of cat №1 is 5.1 g /h (in experiment 2), for cat №2 - 8.3 g /h (experiment 9). In this case, the yield of nanocarbon is 3.3 g /g and 13.4 g /g, respectively.

Figure 8 shows the change in the concentration of active centers along the length of the apparatus for each of the catalysts in experiments 9 (Table 2) at the steady state of the process.

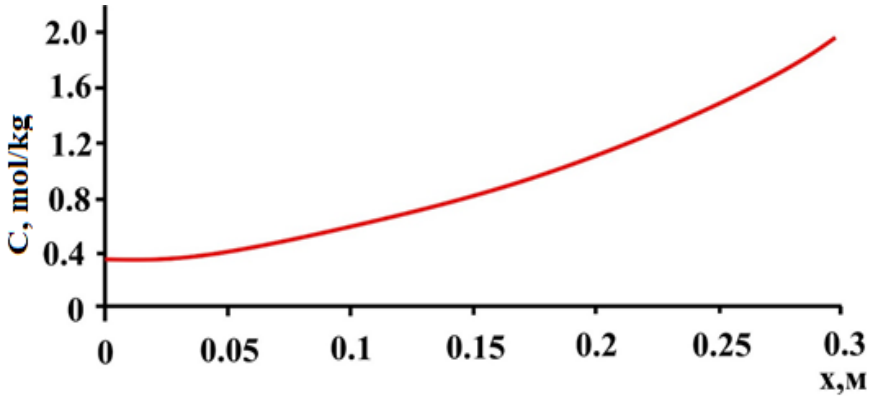

Figure 8. Active centers on the catalyst surface along the length of the reactor change in concentration, mol / kg: cat №2 (Experiment 9).

The curve shown in Figure 8a is an almost straight line. This suggests that cat №1 active sites are consumed continuously throughout the entire process. The slope of this line characterizes the rate of consumption of the active centers of the

catalyst and indicates that this figure is low. The change in the concentration of active centers on the surface of the cat №2 (Fig. 8b) has a clear curvilinear character. At the beginning of the process, the rate of consumption of the active centers of this catalyst is high and significantly exceeds the rate of consumption of the active centers of cat №2. As the catalyst passes from the reactor to the exit point, the rate of consumption of the active centers of cat №2 decreases, and the rate of cat ida1 at the output of the apparatus is close. In general, the cat №2 catalyst is used more efficiently in the methane pyrolysis process.

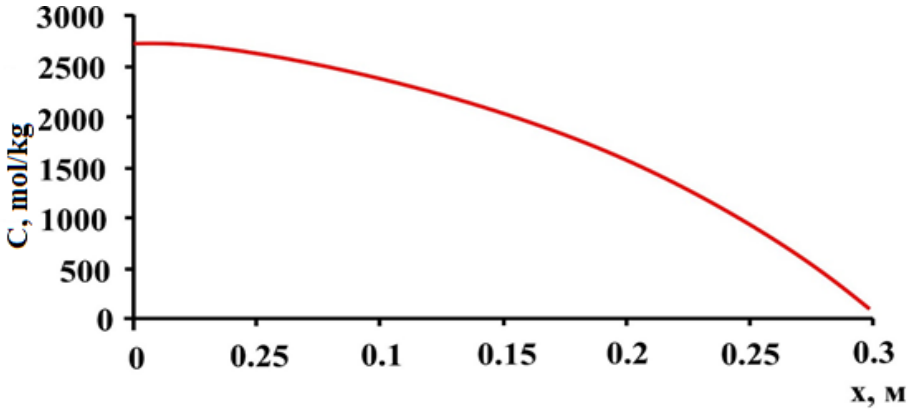

Figure 9. Variation of carbon concentration in the form of nanotubes on the surface of the catalyst along the length of the reactor, mol /kg: cat №2 (Experiment 9).

Figure 9 shows the concentration of nanotubes along the length of the reactor for experiments 2 and 9. As can be seen from Figure 9, the curve has an S-shaped appearance due to the presence of an induction circuit. This is also consistent the results of the kinetic studies of the catalyst kat1, in which the kinetic curves recorded in the solid catalyst layer also include the induction period. The process of nanotube formation in the cat №2 catalyst (Fig. 9) proceeds at a speed close to the maximum almost immediately after the catalyst enters the reactor, which once again demonstrates the efficiency of this catalyst.

Optimization of methane catalytic pyrolysis reactor. In determining the optimal conditions for the synthesis of methane in the catalytic pyrolysis reactor, it is important to determine the acceptance criteria and control parameters. The peculiarity of the nanocarbon production process is that the catalyst is consumed

during the process. That is, the catalyst consumption is high with the low productivity of the nanocarbon, which does not allow the product to achieve a low cost. Therefore, it is important to take into account both nanocarbon output and reactor performance when selecting synthesis conditions.

Process temperature and catalyst flow rate were taken as control parameters. In the calculations, the linear velocity of the gas phase was assumed to be 35 cm /min.

As mentioned above, a series of experiments were performed to find the optimal values of process temperature and catalyst consumption. As a result, it was proved that the dependence of the final product efficiency and productivity on the consumption of the catalyst is of a different nature.

Thus, it is not difficult to determine the optimum temperature of the process with the constant flow rate of the catalyst, because the maximum operation of the reactor and the output of the nanocarbon are achieved at the same temperature. Maximum yield and efficiency are achieved at different values of the process temperature when the consumption of the catalyst changes (Figure 9).

Table 2

Different modes of nanocarbon synthesis from methane

№	Temperature ^{0}C	Catalyst consumption, g/h	Yield of nanocarbon, g/g (%)	Nanocarbon consumption in the reactor, g/h (%)
cat №2				
1	550	0,05	69 (100%)	3,45(20,5%)
2	710	0,8	9,33(13,5%)	16,8(100%)
3	630	0,24	32 (46,5%)	7,8 (46,5%)

CONCLUSION

1. The effect of various factors (catalyst layer thickness, gas phase linear velocity, and process temperature) on the product yield of the methane nanocarbon reaction

from methane was studied.

2. Experimental values of specific gravity and efficiency of a reactor with continuous nanocarbon synthesis in cat №2 catalysts were obtained.

3. A mathematical model of nanocarbon formation during the catalytic pyrolysis of methane in a reactor with a mobile catalyst layer has been developed. This model allows one to determine the composition of nanocarbon and other surface compounds on the surface of the catalyst, the composition of the gas phase at any point in the apparatus, and the flow rate of each stage of the process.

4. From the kinetic scheme of Table 1, the developed mathematical model of a moving catalyst bed reactor was calculated using the kinetic constants selected for the two different catalysts and showed the compatibility of the experimental data.

5. The optimization results show the advantage of cat №2 catalyst in ensuring high values of nanofiber carbon yield and reactor performance.

REFERENCES

1. Bobomurodova, S.Y., Fayzullaev, N.I., Usmanova, K.A. Catalytic aromatization of oil satellite gases//International Journal of Advanced Science and Technology, 2020, 29(5), стр. 3031–3039.
2. Fayzullaev, N.I., Bobomurodova, S.Y., Avalboev, G.A. Catalytic change of C_1-C_4-alkanes//International Journal of Control and Automation, 2020, 13(2), стр. 827–835.
3. Mamadoliev, I.I., Fayzullaev, N.I., Khalikov, K.M. Synthesis of high silicon of zeolites and their sorption properties//International Journal of Control and Automation, 2020, 13(2), стр. 703–709.
4. Mamadoliev, I.I., Fayzullaev, N.I.Optimization of the activation conditions of high silicon zeolite//International Journal of Advanced Science and Technology, 2020, 29(3), стр. 6807–6813.

5. Omanov, B.S., Fayzullaev, N.I., Musulmonov, N.K., Xatamova, M.S., Asrorov, D.A. Optimization of vinyl acetate synthesis process//International Journal of Control and Automation, 2020, 13(1), стр. 231–238.
6. Fayzullaev, N.I, Bobomurodova, S.Y, Xolmuminova, D.A.//Physico-chemical and texture characteristics of Zn-Zr/VKTS catalyst. Journal of Critical Reviews, 2020, 7(7), стр. 917–920.
7. Hilola N. Xolmirzayeva[1], Normurot I. Fayzullayev[2] Obtaining Nanocarbon from Local Raw Materials and Studying Its Textural and Sorption Properties//IJETT, 70(2), 2022, 163-171
8. Katarzyna Lewicka Activated carbons prepared from hazelnut shells, walnut shells and peanut shells for high CO_2 adsorption// Polish Journal of Chemical Technology, 2017, 38 – 43
9. S. Suhdi, Sheng-Chang Wang The Production of Carbon Nanofiber on Rubber Fruit Shell-Derived Activated Carbon by Chemical Activation and Hydrothermal Process with Low Temperature// Nanomaterials 2021, 11, 2038
10. Hilola N. Xolmirzayeva Characteristics of the $Fe_2(MoO_4)_3$*MoO_3 catalyst used in the synthesis of nanocarbons from methane// ACADEMICIA: An International Multidisciplinary Research Journal, 2021, 598-605
11. Wenming Hao, Weimin Zhang, Zaibin Guo, Jinghong Ma Mesoporous Beta Zeolite Catalysts for Benzylation of Naphthalene: Effect of Pore Structure and Acidity// Catalysts 2018, 8, 504
12. Dongdong Xu, Hao Lv and Ben Liu Encapsulation of Metal Nanoparticle Catalysts Within Mesoporous Zeolites and Their Enhanced Catalytic Performances: A Review // Front. Chem., 09 November 2018
13. M.Hadian, K.A.Buist, A.N.R.Bosb, A.M.Kuipers Single catalyst particle growth modeling in thermocatalytic decomposition of methane Chemical Engineering Journal // Volume 421, Part 1, 1 October 2021, 129759

14. K. Srilatha, D.Bhagawan, S.Shiva Kumar, V.Himabindu Sustainable fuel production by thermocatalytic decomposition of methane – A review//South African Journal of Chemical Engineering, 2017, 24, 156-167
15. E. Välimäki, L. Yli-Varo, H. Romar Carbons Formed in Methane Thermal and Thermocatalytic Decomposition Processes: Properties and Applications//Journal of Carbon Research 2021, 7(3), 50
16. S. Grigorievich, Z.G. Kuvshinov Mathematical modeling of continuous production of carbon nanofibers from methane in a reactor with a moving bed of a nickel-containing catalyst // Theoretical Foundations of Chemical Engineering 2006, 40(5), 519-525
17. A. Awad, I. Ahmed, D. Qadir, M. S. Khan, A. Idris Catalytic Decomposition of 2% Methanol in Methane over Metallic Catalyst by Fixed-Bed Catalytic Reactor //Energies 2021, 14, 2220
18. C. A. Schwengbera, F. A. da Silvac, R. A. Schaffner Methane dry reforming using Ni/Al2O3 catalysts: Evaluation of the effects of temperature, space velocity and reaction time// Journal of Environmental Chemical Engineering 4 (2016), 3688–3695
19. D. Micale, R. Uglietti, M. Bracconi, M. Maestri Coupling Euler–Euler and Microkinetic Modeling for the Simulation of Fluidized Bed Reactors: an Application to the Oxidative Coupling of Methane// Industrial & Engineering Chemistry Research, 2021, 60, 18, 6687–6697
20. D. Micale, C. Ferroni, R. Uglietti, M. Bracconi Computational Fluid Dynamics of Reacting Flows at Surfaces: Methodologies and Applications// Chem. Ing. Tech.2022,94, No. 5, 1–19